Short Title : The human disconnectome

Brain disconnections link structural connectivity with function and behaviour

Michel Thiebaut de Schotten[1,2*], Chris Foulon[3], Parashkev Nachev[3]

[1] Brain Connectivity and Behaviour Laboratory, Sorbonne Universities, Paris, France

[2] Groupe d'Imagerie Neurofonctionnelle, Institut des Maladies Neurodégénératives-UMR 5293, CNRS, CEA University of Bordeaux, Bordeaux, France

[3] Institute of Neurology, UCL, London, WC1N 3BG, UK

*Corresponding author: michel.thiebaut@gmail.com

Short Title : The human disconnectome

Abstract

Brain lesions do not just disable but also disconnect brain areas, which once deprived of their input or output, can no longer subserve behaviour and cognition. The role of white matter connections has remained an open question for the past 250 years. Based on 1333 stroke lesions we reveal the human Disconnectome and demonstrate its relationship to the functional segregation of the human brain. Results indicate that functional territories are not only defined by white matter connections, but also by the highly stereotyped spatial distribution of brain disconnections. While the former has granted us the possibility to map 590 functions on the white matter of the whole brain, the latter compels a revision of the taxonomy of brain functions. Overall, our freely available Functional Atlas of the White Matter will enable improved clinical-neuroanatomical predictions for brain lesion studies and provide a platform for novel explorations in the domain of cognition.

Science relies on observation to elaborate theories and models of the nature and behaviour of natural things [1]. Observers notice pieces of evidence haphazardly, or manipulate their environment to produce new perceptible results. However, theories and models can be biased by the deceptive aspect of perception [2] and the incompleteness of data. For instance, unobservables cannot be detected, and are epistemically unavailable [3].

Neuroscience is no different, our understanding of function within the human brain is largely based upon on the observation of patients with focal brain lesions [4, 5], particularly stroke which amputates a part of the mind and impacts one person out of six [6]. Through patient observation, principal functions such as perception [7], emotion [8], memory [9], attention [10] and verbal communication [11] have been identified, localised and subsequently fractionated into more specific cognitive subprocesses. However, brain lesions, especially from ischemic stroke, the most frequent kind [12], are not distributed randomly [13] (Figure 1a) and may have partially biased our taxonomy of brain functions.

In the past 20 years, following Meynert's original insight [14] our understanding of the functioning of the brain has evolved from a fractionated entity to an interconnected unity [15, 16]. Brain zones considered critical to function have slowly altered over time, from those visibly damaged [17, 18] to more distant, long-range zones that were disconnected [19, 20]. Recent data even indicates that white matter disconnection might be a better predictor of brain dysfunction and recovery than the location of the lesion itself [21-23]. While our understanding of the anatomo-functional division of the brain surface is quite advanced [24, 25], the relationship between brain disconnection and dysfunction remains limited and, accordingly, little is known about the functional division of white matter connections in the human brain [16].

Neuroimaging, particularly diffusion-weighted imaging tractography, now enables the estimation of white matter disconnection after a brain lesion (i.e. disconnectome, Figure 1a, [26]). Joint models of lesions and their estimated disconnections both cohere with task-related activations from functional imaging and better explain clinical profiles [19, 26-28]. However, whether the relationship between brain lesion and

functional imaging findings is driven by biased clinical observation or the non-stochastic organisation of white matter connections in the human brain is unknown.

Taking advantage of an extensive set of 1,333 real stroke lesions paired with a synthetic set of randomly distributed artificial lesions of the same size and lateralisation (Figure 1b) we used a machine learning algorithm (i.e. T-distributed Stochastic Neighbor Embedding, T-SNE, [29]) to visualise the redundancy existing within the distribution of brain lesions (Figure 1c) and their subsequent estimated disconnections (Figure 1d). The result indicates, as previously shown [13] that brain lesions show some redundancy and cluster together more than synthetic lesions (Figure 1c). Importantly, disconnections in strokes (i.e. stroke disconnectome) demonstrated a higher level of clustering in comparison to the disconnection that was derived from paired synthetic lesions (i.e. synthetic disconnectome; Figure 1d).

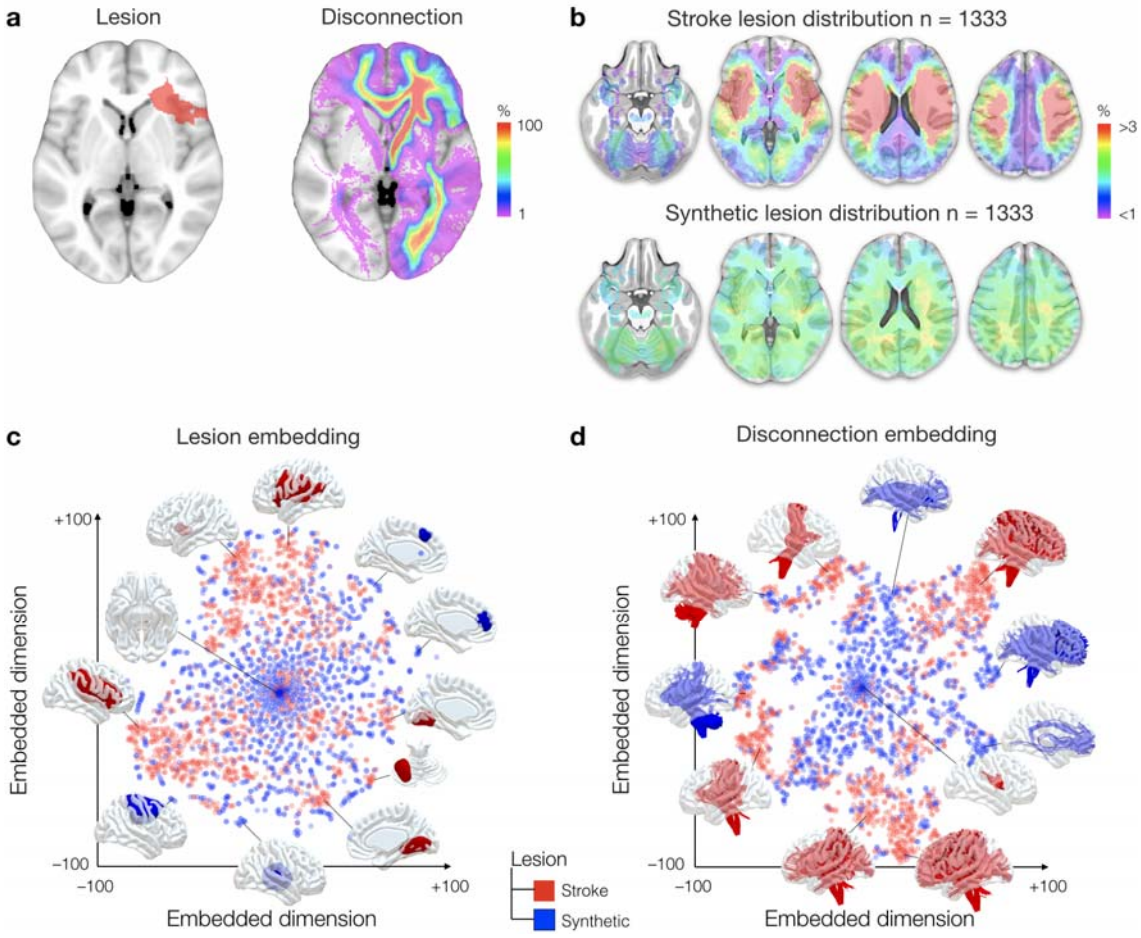

Figure 1: The biased distribution of ischemic stroke. The figure shows (a) a representative brain lesion (left) together with its estimated disconnections (right) (b) the stroke lesion distribution (top row) compared with the synthetic lesion distribution (bottom row), (c) the two-dimension space visualisation of stroke (red) and synthetic lesion (blue) distribution and (d) the two-dimension space visualisation of stroke (red) and synthetic disconnectome (blue) distribution.

Redundancy in these datasets suggests that we should be able to summarise the pattern of brain areas disconnected by strokes into principal components.
In order to do so, the pattern of brain areas that were disconnected in each stroke was first characterised by measuring the average level of disconnection in subcortical areas [16] as well as in areas derived from a multimodal atlas of the brain surface [24]. Using a varimax rotated principal component analysis we modelled the main profiles of brain disconnections and revealed that 30 components, out of 46 in total, explained more than 90% of the variance of the regions disconnected by a stroke (Figure 2a). All components were relatively independent from the lesion size (all $R^2 < 0.1$; see supplementary table 1 for a full list of the 46 components pattern of disconnection). In comparison, principal component analysis of the direct lesion and the disconnection derived from the synthetic dataset only explained 70% and 80% of the variance with 30 components (Figure 2a).

In order to assess the relationship between disconnection and brain function, the probability of disconnection of each component was compared to a manually curated version of the most extensive fMRI meta-analytic dataset available [25, 30]. Strikingly, 40 out of the 46 components disconnected a set of brain regions that significantly correlated with a set of specific task-related fMRI meta-analytic maps (Figure 2b) with a small to large effect size (all $r > 0.202$, significant after Bonferroni correction for multiple comparisons; see supplementary material for a full description of all correlations).

Whether the correspondence between the disconnectome components and task-related functional activations was due to the pure organisation of white matter in the brain or was influenced by the biased distribution of ischemic strokes is unknown. To answer this question, we compared the correlation between task-related fMRI meta-

analytic maps and all components of the stroke disconnectome, the synthetic disconnectome, and brain lesions. Figure 2c shows disconnections in strokes have a stronger relationship with task-related functional activations than the lesion alone ($t = 24.107$; $p < 0.001$, based on 1000 bootstrapped samples). Further, the correlation between task-related functional activations and the synthetic disconnectome have a significantly weaker relationship than with the stroke disconnectome ($t = 4.620$; $p < 0.001$, based on 1000 bootstrapped samples). These statistical differences suggest that on the one hand, the disconnectome corresponds with the underlying functional architecture (as revealed by fMRI) better than lesions alone, but on the other, the non-random distribution of stroke has distorted the taxonomy of brain function used in task-related fMRI.

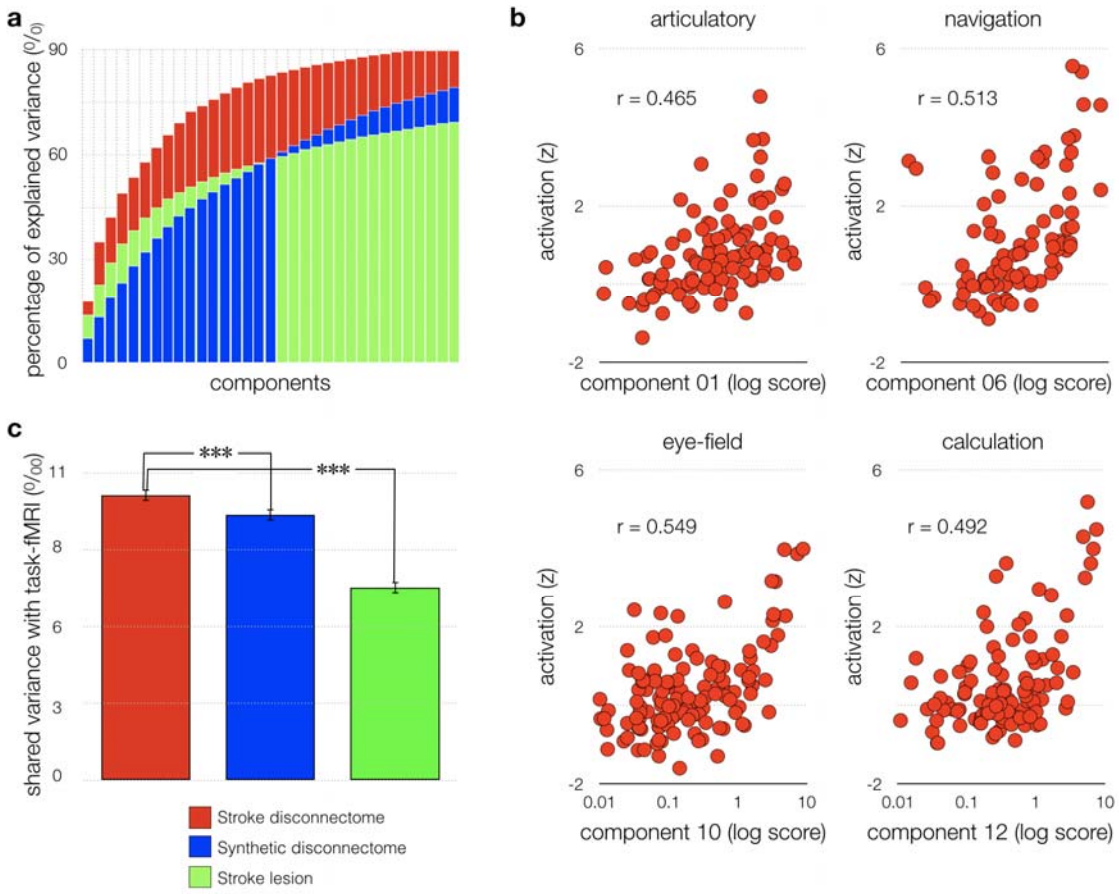

Figure 2: Principal components of stroke and their relationship to function. (a) the cumulative percentage of explained variance for the first 30 components of the stroke disconnectome (red), synthetic disconnectome (blue) and stroke lesion

distribution (green) ; (b) 4 representative examples of the correlation between stroke disconnectome components and task-related functional MRI meta-analytic activations ; (c) average percentage of variance explained by task-related functional MRI meta-analytic activations for the stroke disconnectome (red), synthetic disconnectome (blue) and stroke lesion distribution (green). *** $p < 0.001$. Error bars indicate 95% confidence intervals.

Since most of the disconnectome components corresponded to task-related functional activations, we estimated the white matter structure subjacent to each component allowing to derive, for the first time, a statistical map of the function of white matter connections [as disrupted by stroke]. Accordingly, component maps were calculated using permuted (n = 1000) linear regressions. In order to assess the reproducibility of the component maps, we split the dataset in two (n = 666). Pearson correlation indicated a good reproducibility across the two sets of component maps (average Pearson R = 0.813 +/– 0.079). As shown in figure 3, some components clearly demonstrated an intra-hemispheric network distribution, such as the articulatory loop that involves portions of the arcuate fasciculus and connects key territories including the Broca, supramarginal and Wernicke areas [31]. Similarly, the navigation system involved the posterior portion of the cingulum that connects the right hippocampus [32] to the retrosplenial cortex [33, 34]. Other components appeared to have a strong level of interhemispheric interaction, such as the left and right frontal eye fields that were bound via a portion of the corpus callosum tract. Such a strong interhemispheric association might explain why after a stroke [35] or unilateral electrical stimulation [36] of this functional field both eyes show an irrepressible deviation. Some components also had a more circumscribed distribution, such as calculation, which involved the left intraparietal sulcus and its subjacent short white matter connections, as previously discussed in [37]. See supplementary material for a full description of all the components, their link with functional neuroimaging and with symptoms when disconnected.

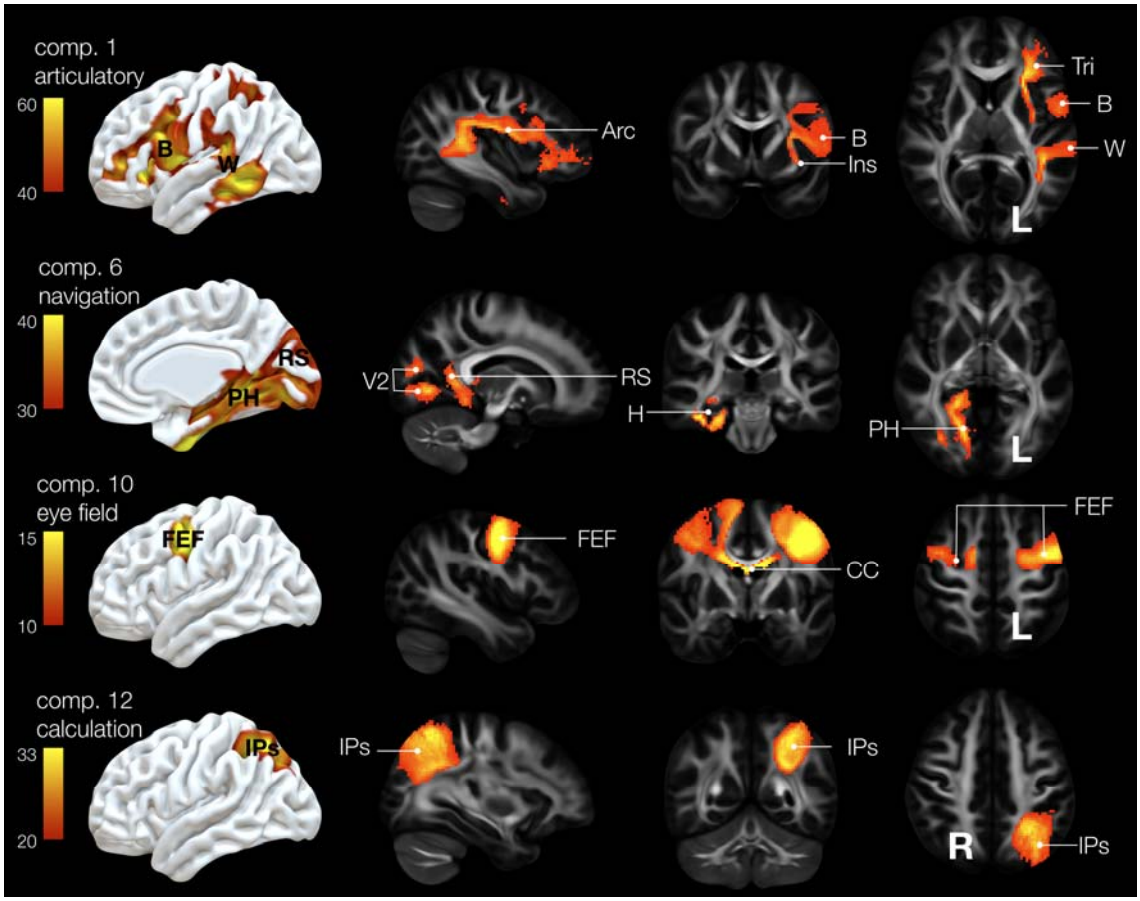

Figure 3: Functional mapping of white matter connections. 3D representation of 4 representative components maps side-by-side with white matter sections. comp.: Component, Arc: Arcuate, B: Broca area, Ins, insula, Tri: pars triangularis, W: Wernicke, V2: secondary visual area, RS: retrosplenial cortex, H: hippocampus, PH: parahippocampal area, FEF: frontal eye field, CC: corpus callosum, IPS, intraparietal sulcus.

As some functions might emerge from the combination of the above components rather than a single component, a second level of permuted linear regression was performed to identify the statistical contribution of each voxel of each component map (i.e. independent variables) to each of the fMRI meta-analytic maps (i.e. the dependant variable). By doing so we obtained a white matter map that corresponded to each fMRI meta-analytic map. The same analysis was replicated in the second set of component maps. The two sets of maps indicated a good level of reproducibility (average Pearson R = 0.885 +/– 0.061). Results are summarised in figure 4a, which shows the first comprehensive atlas of the function of white matter connections. For

visualisation purposes, only the top contribution is represented here, however individual maps are available as supplementary data. Mapping of the effect sizes (figure 4b) and the task versatility (figure 4c) indicated a strong asymmetry between the left and the right hemisphere. This asymmetry suggested that much less is known about the white matter function of the right hemisphere in comparison with the left. Additionally, the component maps made available as supplementary material have the potential to project any functional activation to the white matter and identify typical brain lesions leading to its disconnection (see supplementary material for an example with left hand and right hand finger tapping).

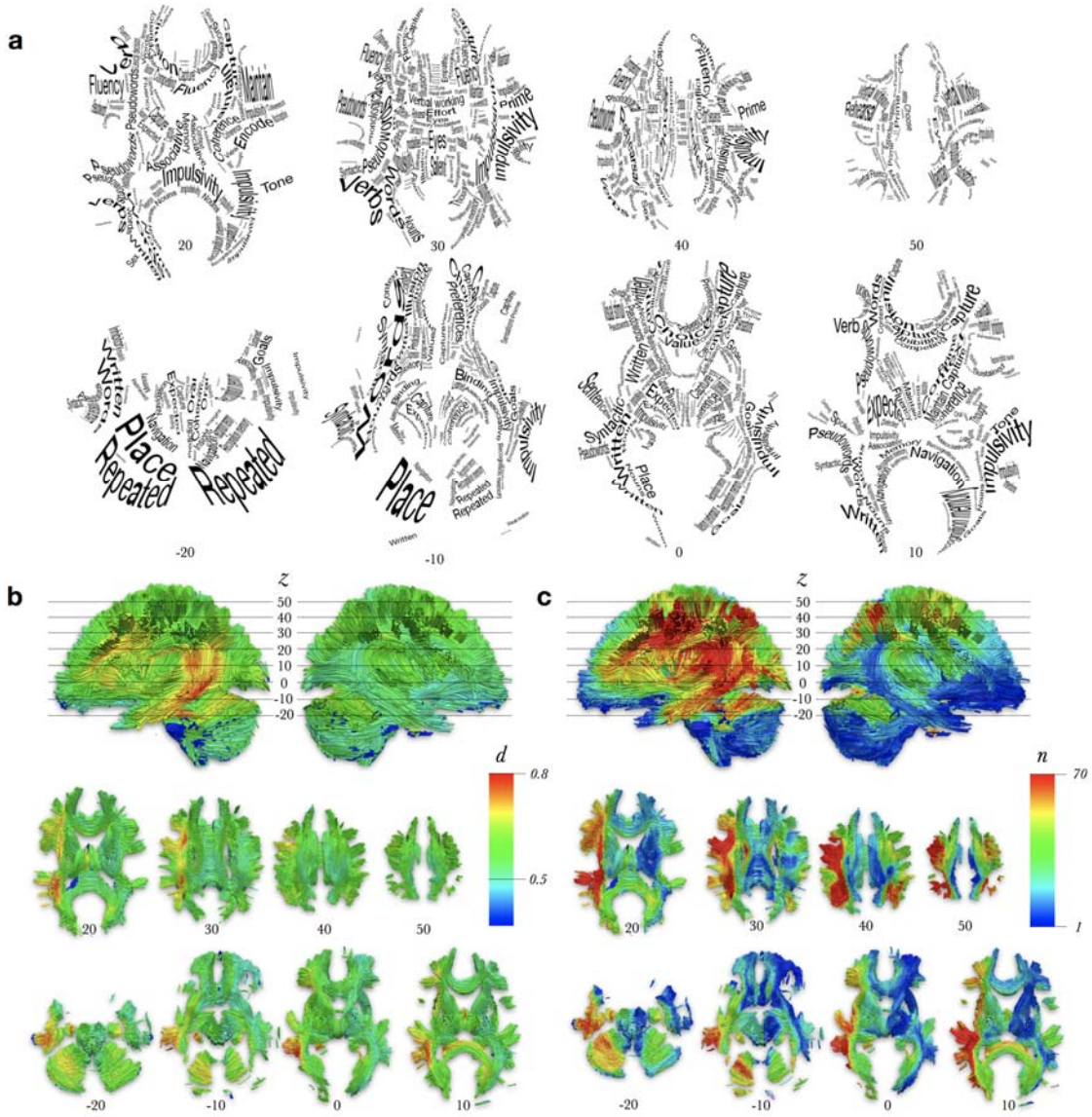

Figure 4: Atlas of white matter function. (a) summary map of the white matter function only displaying terms with the highest statistical level. (b) Effect size related to the prediction of white matter function. Cohen d > 0.5 and d > 0.8 indicates a medium and large effect size respectively. (c) Versatility maps. For each voxels of the MNI, the value indicates the number of terms related to the prediction of white matter function with a medium to large effect size.

In conclusion, applying state-of-the-art methods for synthesising meta-analytic functional mapping with white matter connectivity to the largest published set of acute stroke lesions we built the first atlas of the function of white matter in the human brain. The functions we localised in this atlas correspond to the joint contribution of connected areas. This was made possible because of the redundancy in brain disconnection after a stroke that shows a striking correspondence with task-related fMRI activation patterns. Our result suggests that this correspondence is due to the influence of the organisation of white matter connections on the functional segregation of the human brain. Since the relationship between disconnection and task-related fMRI activation patterns was significantly stronger for real stroke lesion than simulated lesions, we suggest that the biased distribution of brain lesions has also biased our taxonomy of brain functions. While our method allowed us to map for the first-time white matter function and may help to guide patients' symptoms exploration, the bias we report also provokes questioning and further investigation on the definition of brain functions, especially within the right hemisphere.

Methods

The following workflow was summarised in supplementary figure 1.

Stroke lesions

The lesions used in this research were derived from human ischemic strokes brain lesion maps (n = 1333), non-linearly registered to the Montreal neurological institute space (2*2*2 millimetres MNI; http://www.bic.mni.mcgill.ca) so as to allow direct comparisons across individuals. Data were routinely acquired in the clinic and were anonymised prior to analysis and their collection was approved and monitored by the UK Health Research Authority. See [38] for further details.

Synthetic lesions

To assess the impact of the spatial distribution of stroke lesion we computed synthetic lesions paired in size and hemispheric lateralisation with the stroke lesion dataset. To do so, we repeatedly divided each hemisphere of the brain mask of all the stroke lesions using k-mean clusterings [39] applied to the coordinates of each voxel varying the number of clusters from 2 to 50000. This produced more than 1 million synthetic lesion masks. In order to minimise the bulkiness of the synthetic lesion, each mask was subsequently smoothed with a full-width half-maximum of 10 mm, thresholded at 0.3 and binarized. Finally, for each lesion of the stroke dataset, we sampled a lesion of the synthetic pool with the same size and localised in the same hemisphere. This produced a dataset of 1333 synthetic lesions exactly paired with the stroke dataset but pseudo-randomly distributed in the brain.

Disconnectome

Similarly to previous work [19, 26, 40] the probability of disconnection induced by each lesion was computed with the 'disconnectome map' tool of the BCBToolkit software [26].

Firstly, we tracked white matter fibres that pass through each lesion in 163 healthy controls tractographies dataset acquired at 7 Tesla by the Human Connectome Project Team [41] and computed according to [30]. For each lesion, tractography maps of the 163 healthy controls were subsequently binarised and averaged together so that each voxel represented a probability of disconnection from 0 to 1. This produced a stroke lesion disconnectome dataset (n = 1333) and a synthetic lesion disconnectome dataset (n = 1333).

Spatial Embedding

Stroke lesions and synthetic lesions, as well as their respective disconnectome maps' spatial distributions, were visually compared using a machine learning visualisation approach, t-distributed Stochastic Neighbor Embedding (t-SNE) [29]. t-SNE provided a 2-dimensional visualisation of the similarity and difference between the maps so that a smaller distance between two points represented a higher

similarity between the maps. T-SNE was computed with scikit learn in Python 3 with a perplexity of 30, an exaggeration of 12 (to increase the space between clusters) a learning rate of 200 and 1000 iterations. This step provided us with the visualisation of the stroke and synthetic lesions and disconnectome map distribution that is displayed in figure 1a and 1b.

Data Compression

In order to properly deal with redundancy, lesions and disconnectome of the stroke and the synthetic datasets were first characterised using the multimodal parcellation of human cerebral cortex (MMP, [24]) and subsequently entered a varimax-rotated Principal Component Analysis (PCA).

The MMP provided 360 cortical areas very well characterised by their anatomy and functional specificity. As subcortical areas also play an important role in cognition we added 12 additional regions, defined manually, including the amygdala, the caudate nucleus, the hippocampus, the pallidum, the putamen and the thalamus for the left and the right hemispheres, respectively.

For each lesion, the proportion of damage (for the lesions) or the probability of disconnection (for the disconnectome) was estimated for each region of interest. This step produced 4 matrices in total—2 (lesion or disconnectome) x 2 (stroke or synthetic).

Each matrix entered a PCA using a covariance matrix and varimax rotation (with a maximum of 500 iterations for convergence) in order to estimate the number of principal components to extract for the 4 conditions (Fig. 1). Plot of the components according to their cumulative explained variance can be seen in Figure 2a. Component scores were systematically extracted for all components identified by the PCA by means of multiple regression. This provided us with the contribution of each parcel of the MMP and subcortical areas to each components.

Relationship to task-related fMRI metanalysis

We used a meta-analytic database [25] (http://Neurosynth.org) that summarises the details of 11,406 *f*MRI literature sources and manually curated it as described in [30].

The curated database represented 590 cognitive term maps that were converted into a matrix using the average z value for each MMP parcels and the manually defined subcortical areas mentioned above.

We estimated the relationship between each term of the task-related *f*MRI metanalysis matrix and the component scores extracted in the previous section using Pearson correlation.

Comparison between the stroke lesion, disconnectome and synthetic disconnectome relationship with task-related fMRI metanalysis was assessed by means of a bootstrapped (n = 1000) independent t-test.

Components maps

We used a permuted (n = 1000) multiple regression to statistically assess the relationship between each component and voxel in the white matter. To do so, we used the component score as an independent variable and the voxel probability of disconnection in the stroke disconnectome maps as dependant variables. This analysis was made possible thanks to the function *Randomise* as part of the software package FSL (https://fsl.fmrib.ox.ac.uk/fsl [42, 43]).

To address the replicability of our maps, the 1333 disconnectome maps dataset was split in two 666 datasets and the multiple regression was run twice. Quality of the results duplication was assessed by means of Pearson correlations between the two set of maps derived from the analyses. This section resulted in two white matter maps per component.

Atlas of the white matter function

Next, we explored the contribution of each component map voxels to the task-related fMRI meta-analytic maps. A permuted (n = 1000) linear regression was computed between the correlation value of each task-related fMRI meta-analytic map as an independent variable and each component maps voxels as a dependant variable. This analysis was run twice, once for each set of the component maps and its replication quality was assessed as previously mentioned. This section resulted in two white matter maps per task-related fMRI meta-analytic terms.

A summary map of the white matter function was computed displaying only the map with the highest statistical level (*find_the_biggest* in FSL). A Cohen *d* was calculated

for each voxel in order to provide a visualisation of the effect size of the summary map. As several functions can load on the same tract, we assessed versatility by counting the number of tasks having an effect size d > 0.5 for each voxel.

Visualisation

A visualisation of the results was performed using Surf Ice https://www.nitrc.org/projects/surfice/ and Trackvis http://trackvis.org

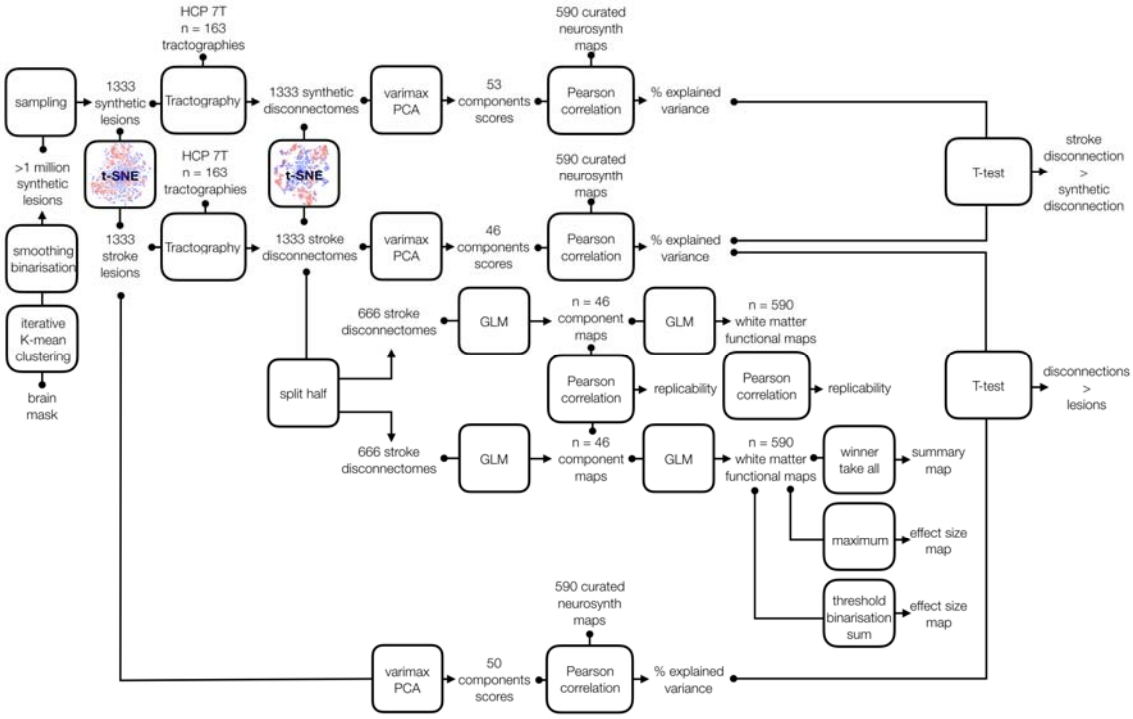

Supplementary figure 1: Graphical summary of the neuroimaging workflow

Acknowledgements

We thank Tianbo Xu, who generated all the stroke lesion masks and Lauren Sakuma for useful discussion and edits to the manuscript. We thank Maurizio Corbetta, Stephanie Forkel, Emmanuelle Volle, Patrick Friedrich and Sandrine Cremona for discussion of the results. We also thank Laurent Petit and his team (GIN) for providing us with fMRI maps of left and right hands finger tapping. This project has received funding from the European Research Council (ERC) under the European Union's Horizon 2020 research and innovation programme (grant agreement No.

818521 to MTS). PN is funded by the Wellcome Trust and the UCLH NIHR Biomedical Research Centre.

Authors contribution statement

M.T.S. conceived and coordinated the study, implemented the methods, performed the analyses, wrote the manuscript and provided funding. C.F. implemented the methods and wrote the manuscript. P.N. conceived and coordinated the study, collected and reviewed the neuroimaging data, wrote the manuscript and provided funding.

Data and Code availability

The two set of component maps and the atlas of white matter function (original and replication) are available as supplementary data with the manuscript.
The raw dataset analysed in the current study are available at https://www.humanconnectome.org (7T diffusion data), http://www.neurosynth.org (metanalytic functional MRI maps). In addition, processed data are available on request to the corresponding author michel.thiebaut@gmail.com.
The code used in the analyses is available as part of the BCBtoolkit package http://toolkit.bcblab.com and on request to michel.thiebaut@gmail.com

References

1. Bacon, F. *Novum Organum with other parts of the Great Instauration* (1620).
2. Searle, J.R. *Seeing things as they are* (Oxford University Press, New York, 2015).
3. Bogen, J. & Woodward, J. Saving the Phenomena. *Philosophical Review* **XCVII**, 303–352 (1988).
4. Damasio, H. & Damasio, A. *Lesion analysis in Neuropsychology* (New York, 1989).
5. Vaidya, A.R., Pujara, M.S., Petrides, M., Murray, E.A. & Fellows, L.K. Lesion Studies in Contemporary Neuroscience. *Trends Cogn Sci* **23**, 653-671 (2019).
6. Kirchhof, P.*, et al.* How can we avoid a stroke crisis? . (2009).
7. Ungerleider, L.G. & Mishkin, M. Two Cortical Visual Systems. in *Analysis of Visual Behavior* (ed. D.J. Ingle, M.A. Goodale & R.J.W. Mansfield) (MIT Press, Boston, 1982).
8. Adolphs, R.*, et al.* A mechanism for impaired fear recognition after amygdala damage. *Nature* **433**, 68-72 (2005).
9. Corkin, S. *Permanent Present Tense: The Unforgettable Life of the Amnesic Patient H.M.* (Basic Books, Philadelphia, 2013).
10. Posner, M.I., Cohen, Y. & Rafal, R.D. Neural systems control of spatial orienting. *Philos Trans R Soc Lond, B, Biol Sci* **298**, 187-198 (1982).
11. Lichtheim, L. On aphasia. *Brain* **7**, 433-484 (1885).
12. Shiber, J.R., Fontane, E. & Adewale, A. Stroke registry: hemorrhagic vs ischemic strokes. *Am J Emerg Med* **28**, 331-333 (2010).

13. Mah, Y.H., Husain, M., Rees, G. & Nachev, P. Human brain lesion-deficit inference remapped. *Brain* **137**, 2522-2531 (2014).
14. Meynert, T. Der Bau der Grosshirnrinde und seine ortlichen Verschiedenheiten, nebst einem pathologisch-anatomischen Corollarium. *Vierteljahresschrift für Psychiatrie*, 77-93 (see also pp. 198-217) (1867).
15. Sporns, O. *Networks of the brain* (MIT Press, Cambridge, Mass., 2011).
16. Catani, M. & Thiebaut de Schotten, M. *Atlas of Human Brain Connections* (Oxford University Press, Oxford, 2012).
17. Bates, E.*, et al.* Voxel-based lesion-symptom mapping. *Nature Neuroscience* **6**, 448-450 (2003).
18. Karnath, H.O., Ferber, S. & Himmelbach, M. Spatial awareness is a function of the temporal not the posterior parietal lobe. *Nature* **411**, 950-953 (2001).
19. Thiebaut de Schotten, M.*, et al.* From Phineas Gage and Monsieur Leborgne to H.M.: Revisiting Disconnection Syndromes. *Cereb Cortex* **25**, 4812-4827 (2015).
20. Fox, M.D. Mapping Symptoms to Brain Networks with the Human Connectome. *N Engl J Med* **379**, 2237-2245 (2018).
21. Thiebaut de Schotten, M.*, et al.* Damage to white matter pathways in subacute and chronic spatial neglect: a group study and 2 single-case studies with complete virtual "in vivo" tractography dissection. *Cereb Cortex* **24**, 691-706 (2014).
22. Corbetta, M.*, et al.* Common behavioral clusters and subcortical anatomy in stroke. *Neuron* **85**, 927-941 (2015).
23. Herbet, G., Maheu, M., Costi, E., Lafargue, G. & Duffau, H. Mapping neuroplastic potential in brain-damaged patients. *Brain* **139**, 829-844 (2016).
24. Glasser, M.F.*, et al.* A multi-modal parcellation of human cerebral cortex. *Nature* **536**, 171-178 (2016).
25. Yarkoni, T., Poldrack, R.A., Nichols, T.E., Van Essen, D.C. & Wager, T.D. Large-scale automated synthesis of human functional neuroimaging data. *Nat Methods* **8**, 665-670 (2011).
26. Foulon, C.*, et al.* Advanced lesion symptom mapping analyses and implementation as BCBtoolkit. *Gigascience* **7**, 1-17 (2018).
27. Boes, A.D.*, et al.* Network localization of neurological symptoms from focal brain lesions. *Brain* **138**, 3061-3075 (2015).
28. Ferguson, M.A.*, et al.* A human memory circuit derived from brain lesions causing amnesia. *Nat Commun* **10**, 3497 (2019).
29. van der Maaten, L.J.P. & Hinton, G.E. Visualizing Data Using t-SNE. *Journal of Machine Learning Research*, 2579–2605 (2008).
30. Karolis, V.R., Corbetta, M. & Thiebaut de Schotten, M. The architecture of functional lateralisation and its relationship to callosal connectivity in the human brain. *Nat Commun* **10**, 1417 (2019).
31. Paulesu, E., Frith, C.D. & Frackowiak, R.S. The neural correlates of the verbal component of working memory. *Nature* **362**, 342-345 (1993).
32. O'Keefe, J. & Nadel, L. *The hippocampus as a cognitive map* (Clarendon Press ; Oxford University Press, Oxford
New York, 1978).
33. Mao, D., Kandler, S., McNaughton, B.L. & Bonin, V. Sparse orthogonal population representation of spatial context in the retrosplenial cortex. *Nat Commun* **8**, 243 (2017).
34. Alexander, A.S. & Nitz, D.A. Spatially Periodic Activation Patterns of Retrosplenial Cortex Encode Route Sub-spaces and Distance Traveled. *Curr Biol* **27**, 1551-1560 e1554 (2017).
35. Fruhmann Berger, M., Pross, R.D., Ilg, U. & Karnath, H.O. Deviation of eyes and head in acute cerebral stroke. *BMC Neurol* **6**, 23 (2006).
36. Gould, H.J., 3rd, Cusick, C.G., Pons, T.P. & Kaas, J.H. The relationship of corpus callosum connections to electrical stimulation maps of motor, supplementary motor, and the frontal eye fields in owl monkeys. *J Comp Neurol* **247**, 297-325 (1986).

37. Kleinschmidt, A. & Rusconi, E. Gerstmann meets Geschwind: a crossing (or kissing) variant of a subcortical disconnection syndrome? *Neuroscientist* **17**, 633-644 (2011).
38. Xu, T., Rolf Jager, H., Husain, M., Rees, G. & Nachev, P. High-dimensional therapeutic inference in the focally damaged human brain. *Brain* **141**, 48-54 (2018).
39. Steinhaus, H. Sur la division des corps matériels en parties. *Bull. Acad. Polon. Sci.* **4**, 801–804 (1957).
40. Pacella, V.*, et al.* Anosognosia for hemiplegia as a tripartite disconnection syndrome. *Elife* **8** (2019).
41. Vu, A.T.*, et al.* High resolution whole brain diffusion imaging at 7T for the Human Connectome Project. *Neuroimage* **122**, 318-331 (2015).
42. Smith, S.M.*, et al.* Advances in functional and structural MR image analysis and implementation as FSL. *NeuroImage* **23**, 208-219 (2004).
43. Jenkinson, M., Beckmann, C.F., Behrens, T.E., Woolrich, M.W. & Smith, S.M. Fsl. *Neuroimage* **62**, 782-790 (2012).